Organic Solar Cells Using a High-Molecular-Weight Benzodithiophene–Benzothiadiazole Copolymer with an Efficiency of 9.4%

Jegadesan Subbiah, Balaji Purushothaman, Ming Chen, Tianshi Qin, Mei Gao, Doojin Vak, Fiona H. Scholes, Xiwen Chen, Scott E. Watkins, Gerard J. Wilson, Andrew B. Holmes, Wallace W. H. Wong, and David J. Jones**

Organic photovoltaics (OPVs) offer a compelling option for tomorrow's photovoltaic devices owing to their low-cost, lightweight, mechanical flexibility, solution processability, and potential for large-area device manufacturing.[1] In the past few years, there has been tremendous progress in the performance of these devices owing to the development of new materials, improved device geometries, and metal/organic interfaces.[2] However, improvement in the power conversion efficiency (PCE) of OPVs is still required to push this technology toward commercial applications. Both device geometry and interface properties are critical factors for the fabrication of high performance OPVs.[3,4] OPV devices with an inverted geometry have gained popularity in recent years as the inverted configuration offers better device stability with its air-stable top metal electrode. In some cases, device performance was enhanced as a result of favorable vertical phase separation and concentration of the active layer.[3,5]

It has been demonstrated that interlayers in OPV devices play an important role for efficient charge extraction by minimizing the contact resistance between active layer and metal electrode. In addition, interlayers can act as charge-blocking layers reducing charge recombination and current leakage at bulk heterojunction electrode interfaces.[3,6] Many solution-processable interlayer materials such as metal oxide, conjugated polyelectrolyte, or self-assembled monolayer have been used to enhance the performance of OPVs. For inverted OPVs, the insertion of a fullerene self-assembled monolayer[7] or a cross-linked fullerene film[8] on the ZnO layer has been shown to enable efficient electron extraction by preventing electron-hole recombination at the interface.

In terms of active layer material selection, the most common approach to enhance the performance of OPVs is to use, as the donor material, polymers with broad absorption in the visible spectrum and high absorptivity. These electron donor polymers should also possess a low-lying highest occupied molecular orbital (HOMO) energy level so that the open-circuit voltage (V_{oc}) of the resulting device is maximized when used with an appropriate electron acceptor.[9] While there are many known polymer structures with appropriate frontier orbital energy levels,[10,11] relatively few examples have been reported with PCEs exceeding 9%.[3,7,12] The molecular weight of the polymer has been shown to be extremely important to achieve high performance devices, particularly from the perspective of charge transport and bulk heterojunction microstructure.[13] Herein, we report a copolymer based on thienyl-substituted benzodithiophene (BDT) and benzothiadiazole (BT), synthesized via a Suzuki polycondensation that delivers a material with a molecular weight (M_n > 100 kg mol^{-1}). The addition of an extra alkyl-solubilizing group on the BDT thienyl substituent was expected to improve polymer solubility allowing for higher polymer molecular weights, while modifying polymer steric bulk and polymer alignment. Placing the BT unit directly beside the BDT unit should also enhance interactions between the electron donor and electron acceptor units.[14] Using this new high molecular weight donor–acceptor copolymer poly[4,8-bis(5-(2-ethylhexyl)-4-hexylthiophen-2-yl)-benzo[1,2-b:4,5-b′] dithiophene-benzothiadiazole] (PBDT–BT) with [6,6]-phenyl-C_{71}-butyric acid methyl ester ($PC_{71}BM$) as the active layer, we fabricated inverted solar cells, with a fullerene-modified ZnO interlayer as a cathode contact, that had a high PCE of 9.4%.

The molecular structure of PBDT—BT is shown in **Figure 1**c. The polymer was synthesized by the Suzuki polycondensation of 4,8-bis(5-(2-ethylhexyl)-4-hexylthiophen-2-yl)-2,6-diiodobenzo[1,2-b:4,5-b′]dithiophene and 2,1,3-benzothia-diazole-4,7-bis(boronic acid pinacol ester). The detailed synthetic procedure can be found in the Supporting Information. The four different molecular weight range samples (M_n = 19, 78, 112, and 136 kg mol^{-1}) of the polymer were obtained by solvent extraction of the polymerization reaction mixture. The 19, 78, and 112 kg mol^{-1} polymer fractions were thoroughly characterized using a range of analytical techniques (Note that the 136 kg mol^{-1} fraction was difficult to characterize because of low solution processability). The decomposition temperatures (5% weight loss from thermal gravimetric analysis) for polymer fractions were all at ca. 420 °C and no thermal phase transitions were detected in differential scanning calorimetry (see Supporting Information for details). The photophysical properties

Dr. J. Subbiah, Dr. B. Purushothaman, Prof. A. B. Holmes, Dr. W. W. H. Wong, Dr. D. J. Jones
School of Chemistry, Bio21 Institute, University of Melbourne
30 Flemington Road, Victoria 3010, Australia
E-mail: wwhwong@unimelb.edu.au; djjones@unimelb.edu.au
Dr. M. Chen, Dr. T. Qin, Dr. M. Gao, Dr. D. Vak, Dr. F. H. Scholes, Dr. X. Chen, Dr. S. E. Watkins, Dr. G. J. Wilson, Prof. A. B. Holmes
CSIRO Manufacturing Flagship
Bag 10, Clayton South
Victoria 3169, Australia

DOI: 10.1002/adma.201403080

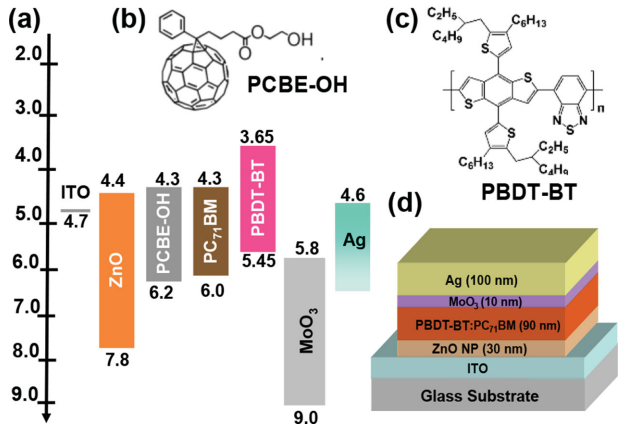

Figure 1. a) Energy level diagram of the components of the inverted device; b) structure of fullerene derivative PCBE—OH; c) structure of low bandgap polymer PBDT—BT, and d) schematic diagram of inverted device geometry.

of the polymer fractions were examined using UV–vis and photoluminescence spectroscopy, and the HOMO energy levels were estimated using both electrochemical and photoelectron spectroscopy in air (PESA) experiments (Table S1, Supporting Information). All polymer fractions showed near identical photophysical properties and the frontier orbital energy levels (HOMO –5.45 eV, LUMO –3.65 eV) of the polymers are illustrated in Figure 1a. The energy levels of the other components of the solar cell device are also shown in Figure 1a. The fullerene interfacial material, [6,6]-phenyl-C_{61}-butyric acid 2-hydroxyethyl ester (PCBE—OH, Figure 1b), was synthesized according to a reported method.[7]

Bulk heterojunction solar cells with inverted geometries were fabricated to assess the performance of the materials (Figure 1d). The polymer active layer and the ZnO layer were deposited by spin coating from 1,2-dichlorobenzene and ethanol, respectively. **Table 1** summarizes the performance characteristics of solar cell devices with various molecular weight of the donor polymer. The values for the best device are shown with average (over 20 devices) and standard deviation in brackets.

A PCE of 4.4% was achieved with the low-molecular-weight polymer (M_n = 19 kg mol^{-1}). When the molecular weight was increased to M_n = 78 kg mol^{-1}, a PCE of 7.6% was obtained. The current density versus voltage (*J*–*V*) curves for devices containing various polymer fractions are shown in Figure S15 (Supporting Information). When the number average molecular weight (M_n) of the polymers increased further, from 78 to 112 kg mol^{-1}, the short circuit current (J_{sc}) and fill factor (FF) increased from 13.6 mA cm^{-2} and 60% to 14.5 mA cm^{-2} and 64%, respectively, resulting in improved PCE from 7.6% to 8.5% (Table 1). A further increase in the molecular weight from 112 to 136 kg mol^{-1} led to a decrease in the PCEs from 8.5% to 6.4%. This decrease was attributed to the poor processability of the highly viscous solution containing the 136 kg mol^{-1} polymer. The higher viscosity solution resulted in changes to active layer thickness and possibly the microstructure of the blend films. These results show that there was an optimum molecular weight range that was necessary to achieve the best device performance, in accord with previous results.[15]

To further enhance the performance of the OPVs, we inserted a thin layer of PCBE—OH between the ZnO layer and the active layer.[7] The optimum polymer fraction (112 kg mol^{-1}) was used in the active layer with $PC_{71}BM$. Detailed information about formation of the fullerene layer on ZnO is given in the Supporting Information. The *J*–*V* characteristics of the photovoltaic devices with and without the PCBE—OH layer are shown in **Figure 2**a. The device performance parameters are listed in Table 1. Compared with the device with ZnO only, the device with ZnO/PCBE—OH layer gave the best device performance with a PCE of 9.4%. This improvement is consistent with enhanced charge extraction due to the PCBE—OH layer at the cathode interface. To verify the enhancement in J_{sc}, we performed external quantum efficiency (EQE) measurements on the devices with and without the PCBE—OH layer. Overall enhancement in the entire absorption range was observed, which was indicative of an increase in current density resulting from efficient charge collection (Figure 2b). From atomic force microscopy experiments, the surface microstructure of both active layers shows the appearance of phase-separated domains with feature size of tens of nanometer, indicating the formation of favorable microstructure in the blend films (Figure S16, Supporting Information).

It was expected that the PCBE—OH layer formed on top of the ZnO by reaction between the hydroxyl group of the fullerene derivative with the ZnO surface. X-ray photoelectron spectroscopy (XPS) analysis revealed a significant increase in the concentration of carbon relative to that of zinc upon coating the ZnO surface with a PCBE—OH layer (C/Zn increased from 0.5 to 2.9), strong evidence for the presence of PCBE—OH. This was confirmed by a comparison of the high resolution C 1 s spectrum before and after coating as shown in **Figure 3**a. Upon coating the ZnO surface with a PCBE—OH layer (2–5 nm), the major C

Table 1. Photovoltaic performance of **PBDT—BT**:$PC_{71}BM$ solar cells.[a)]

M_n/Interlayers	J_{sc} [mA cm^{-2}]	V_{oc} [V]	FF [%]	PCE [%]
19 kg mol^{-1} / ZnO	9.5 (9.3 ± 0.3)	0.92 (0.90 ± 0.02)	50 (49 ± 3)	4.4 (4.25 ± 0.30)
78 kg mol^{-1} / ZnO	13.6 (13.4 ± 0.3)	0.92 (0.92 ± 0.01)	60 (60 ± 2)	7.6 (7.40 ± 0.30)
112 kg mol^{-1} / ZnO	14.5 (14.3 ± 0.2)	0.92 (0.92 ± 0.01)	64 (62 ± 2)	8.5 (8.45 ± 0.25)
136 kg mol^{-1} / ZnO	13.4 (13.1 ± 0.3)	0.90 (0.90 ± 0.02)	53 (51 ± 3)	6.4 (6.20 ± 0.30)
112 kg mol^{-1} / ZnO / PCBE—OH[b)]	15.4 (15.4 ± 0.7)	0.92 (0.92 ± 0.01)	66 (64 ± 3)	9.4 (9.15 ± 0.35)

[a)]Average values and standard deviation of device statistics from 20 devices are given in parentheses; [b)]Average of 80 devices.

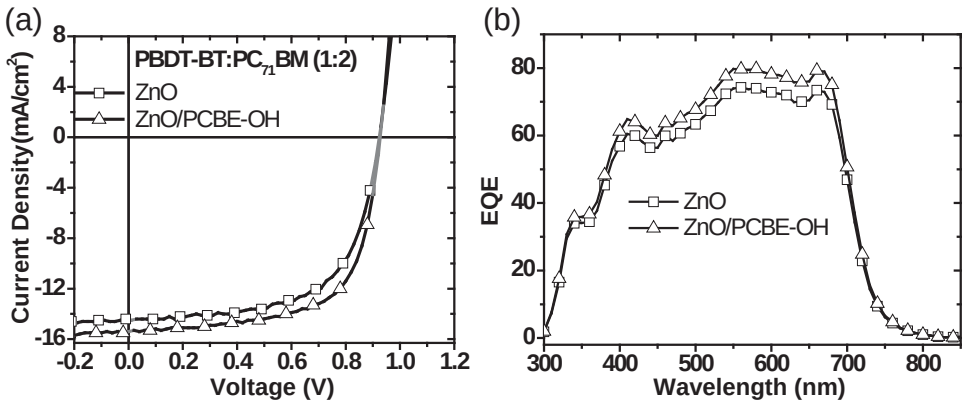

Figure 2. a) *J–V* curves and b) EQE spectra of the BHJ solar cells based on PBDT–BT polymer (M_n = 112 kg m^{-1}) with (triangle) and without (square) PCBE—OH interlayer.

1 s peak at approximately 285.0 eV (C—C, C—H) increased markedly,[16] as would be expected for PCBE—OH. The relative intensity of the Zn 2p peak (Figure S18, Supporting Information), on the other hand, decreased significantly.[17,18] These XPS results indicated that PCBE—OH was present on the ZnO surface.

Another explanation for the enhancement of device performance by the PCBE—OH layer could be due to the elimination of oxygen vacancies on the ZnO surface.[19] Oxygen vacancies on ZnO are defect states that can act as electron traps.[16,18] This ZnO surface passivation was investigated by photoluminescence (PL) measurements. A strong broad emission band at 540 nm was observed for ZnO films that has been assigned to the presence of defect states in ZnO (Figure 3b).[19,20] This emission was effectively quenched when PCBE—OH was deposited on the ZnO. This observation can be explained the elimination of oxygen vacancies in the ZnO.[20] This defect passivation apparently reduced carrier recombination at the ZnO/active layer interface enhancing device performance.

In summary, we have successfully demonstrated highly efficient OPVs with a PCE of 9.4% using a new donor–acceptor copolymer polymer PBDT—BT and $PC_{71}BM$ in the active layer and a modified ZnO-charge extraction layer. The excellent device performance resulted from active layer material optimization and electrode active layer interface engineering. In preliminary studies, further performance enhancement may be possible with selected additives in the active layer blend, these studies are being completed and will be included in a full paper being prepared. In addition, detailed studies on the effect of polymerization methods and various molecular weights of the polymers on the device performance are currently being explored in our laboratory and will be published elsewhere.

Supporting Information

Details on the synthesis of polymer, detailed experimental procedures, and characterization data used in this study are included in the Supporting Information. This material is available from the Wiley Online Library or from the author.

Acknowledgements

This work was made possible by funding to the Victorian Organic Solar Cell Consortium (VICOSC) from the Victorian State Government (DSDBI) and the Australian Renewable Energy Agency (Project 2-A018), the Australian Centre for Advanced Photovoltaics (ACAP).

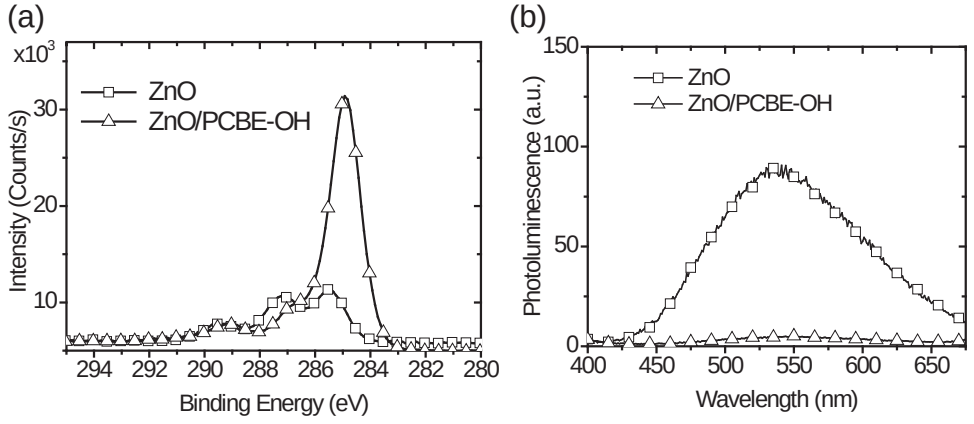

Figure 3. a) XPS analysis of C 1 s spectra recorded at 70° emission angle w.r.t. the surface normal and b) photoluminescence (PL) spectra of the ZnO film with and without PCBE—OH layer (λ_{ex} = 350 nm).

W.W.H.W. is supported by an ARC Future Fellowship (FT130100500) and T.Q. has been supported by fellowships from the CSIRO Office of the Chief Executive and the Australian Renewable Energy Agency. This work was performed in part at the Melbourne Centre for Nanofabrication (MCN) in the Victorian Node of the Australian National Fabrication Facility (ANFF). The authors thank Thomas Gengenbach (CSIRO) for the XPS results.

Received: July 10, 2014
Revised: October 28, 2014
Published online: November 27, 2014

[1] a) B. C. Thompson, J. M. J. Fréchet, *Angew. Chem. Int. Ed.* **2008**, *47*, 58; b) G. Li, R. Zhu, Y. Yang, *Nat. Photonics* **2012**, *6*, 153; c) S. Gunes, H. Neugebauer, N. S. Sariciftci, *Chem. Rev.* **2007**, *107*, 1324; d) F. C. Krebs, *Sol. Energy Mater. Sol. Cells* **2009**, *93*, 394.

[2] a) Y. Liang, Z. Xu, J. Xia, S. T. Tsai, Y. Wu, G. Li, C. Ray, L. Yu, *Adv. Mater.* **2010**, *22*, E135; b) M. Zhang, Y. Gu, X. Guo, F. Liu, S. Zhang, L. Huo, T. P. Russell, J. Hou, *Adv. Mater.* **2013**, *25*, 4944; c) J. You, L. Dou, K. Yoshimura, T. Kato, K. Ohya, T. Moriarty, K. Emery, C.-C. Chen, J. Gao, G. Li, Y. Yang, *Nat. Commun.* **2013**, *4*, 1446; d) J. Subbiah, C. M. Amb, I. Irfan, Y. Gao, J. R. Reynolds, F. So, *ACS Appl. Mater. Interfaces* **2012**, *4*, 866.

[3] Z. He, C. Zhong, S. Su, M. Xu, H. Wu, Y. Cao, *Nat. Photonics* **2012**, *6*, 591.

[4] a) C. E. Small, S. Chen, J. Subbiah, C. M. Amb, S.-W. Tsang, T.-H. Lai, J. R. Reynolds, F. So, *Nat. Photonics* **2012**, *6*, 115; a) H. Ma, H.-L. Yip, F. Huang, A. K. Y. Jen, *Adv. Funct. Mater.* **2010**, *20*, 1371; c) T. Yang, M. Wang, C. Duan, X. Hu, L. Huang, J. Peng, F. Huang, X. Gong, *Energy Environ. Sci.* **2012**, *5*, 8208.

[5] a) Z. Xu, L.-M. Chen, G. Yang, C.-H. Huang, J. Hou, Y. Wu, G. Li, C.-S. Hsu, Y. Yang, *Adv. Funct. Mater.* **2009**, *19*, 1227; b) J. Subbiah, C. M. Amb, J. R. Reynolds, F. So, *Sol. Energy Mater. Sol. Cells* **2012**, *97*, 97; c) S. K. Hau, H.-L. Yip, A. K. Y. Jen, *Polym. Rev.* **2010**, *50*, 474.

[6] a) Y. E. Ha, M. Y. Jo, J. Park, Y.-C. Kang, S. I. Yoo, J. H. Kim, *J. Phys. Chem. C* **2013**, *117*, 2646; b) Y.-J. Cheng, F.-Y. Cao, W.-C. Lin, C.-H. Chen, C.-H. Hsieh, *Chem. Mater.* **2011**, *23*, 1512.

[7] S.-H. Liao, H.-J. Jhuo, Y.-S. Cheng, S.-A. Chen, *Adv. Mater.* **2013**, *25*, 4766.

[8] C.-H. Hsieh, Y.-J. Cheng, P.-J. Li, C.-H. Chen, M. Dubosc, R.-M. Liang, C.-S. Hsu, *J. Am. Chem. Soc.* **2010**, *132*, 4887.

[9] a) S. C. Price, A. C. Stuart, L. Yang, H. Zhou, W. You, *J. Am. Chem. Soc.* **2011**, *133*, 4625; b) T.-Y. Chu, J. Lu, S. Beaupré, Y. Zhang, J.-R. M. Pouliot, S. Wakim, J. Zhou, M. Leclerc, Z. Li, J. Ding, Y. Tao, *J. Am. Chem. Soc.* **2011**, *133*, 4250.

[10] H. Zhou, L. Yang, W. You, *Macromolecules* **2012**, *45*, 607.

[11] X. Guo, N. Zhou, S. Lou, J. Smith, D. Tice, J. Hennek, R. Ortiz, J. Navarrete, S. Li, J. Strzalka, L. Chen, R. Chang, A. Facchetti, T. Marks, *Nat. Photonics* **2013**, *7*, 825.

[12] a) X. Guo, M. Zhang, W. Ma, L. Ye, S. Zhang, S. Liu, H. Ade, F. Huang, J. Hou, *Adv. Mater.* **2014**, *26*, 4043; b) L. Ye, S. Zhang, W. Zhao, H. Yao, J. Hou, *Chem. Mater.* **2014**, *26*, 3603.

[13] T.-Y. Chu, J. Lu, S. Beaupré, Y. Zhang, J.-R. Pouliot, J. Zhou, A. Najari, M. Leclerc, Y. Tao, *Adv. Funct. Mater.* **2012**, *22*, 2345.

[14] A. Facchetti, *Chem. Mater.* **2011**, *23*, 733.

[15] a) J. W. Kingsley, P. P. Marchisio, H. Yi, A. Iraqi, C. J. Kinane, S. Langridge, R. L. Thompson, A. J. Cadby, A. J. Pearson, D. G. Lidzey, R. A. Jones, A. J. Parnell, *Sci. Rep.* **2014**, *4*, 5286; b) C. Müller, E. Wang, L. M. Andersson, K. Tvingstedt, Y. Zhou, M. R. Andersson, O. Inganäs, *Adv. Funct. Mater.* **2010**, *20*, 2124; c) R. S. Ashraf, B. C. Schroeder, H. A. Bronstein, Z. Huang, S. Thomas, R. J. Kline, C. J. Brabec, P. Rannou, T. D. Anthopoulos, J. R. Durrant, I. McCulloch, *Adv. Mater.* **2013**, *25*, 2029.

[16] S. T. Tan, X. W. Sun, Z. G. Yu, P. Wu, G. Q. Lo, D. L. Kwong, *Appl. Phys. Lett.* **2007**, *91*, 72101.

[17] R. Mitsumoto, T. Araki, E. Ito, Y. Ouchi, K. Seki, K. Kikuchi, Y. Achiba, H. Kurosaki, T. Sonoda, H. Kobayashi, O. V. Boltalina, V. K. Pavlovich, L. N. Sidorov, Y. Hattori, N. Liu, S. Yajima, S. Kawasaki, F. Okino, H. Touhara, *J. Phys. Chem. A* **1998**, *102*, 552.

[18] Y.-S. Cheng, S.-H. Liao, Y.-L. Li, S.-A. Chen, *ACS Appl. Mater. Interfaces* **2013**, *5*, 6665.

[19] V. Ischenko, S. Polarz, D. Grote, V. Stavarache, K. Fink, M. Driess, *Adv. Funct. Mater.* **2005**, *15*, 1945.

[20] S. Chen, C. E. Small, C. M. Amb, J. Subbiah, T.-h. Lai, S.-W. Tsang, J. R. Manders, J. R. Reynolds, F. So, *Adv. Energy Mater.* **2012**, *2*, 1333.